CrystEngComm

Accepted Manuscript

ROYAL SOCIETY OF CHEMISTRY

www.rsc.org/crystengcomm

Compositional effects and optical properties of $CdSe_XTe_{1-X}$ alloyed nanotube arrays

Xina Wang,[1, 2] Yang Xu,[1] Rui Tong,[1,] Xiaolong Zhou,[1] Quan Li,[2,*] Hao Wang[1,*]

[1]*Hubei Collaborative Innovation Center for Advanced Organic Chemical Materials, Faculty of Physics and Electronic Technology, Hubei University, Wuhan, Hubei 430062*

[2]*Department of Physics, The Chinese University of Hong Kong, Shatin, New Territory, Hong Kong, China,*

Abstract:

Well-aligned $CdSe_XTe_{1-X}$ nanotube arrays with X valued from 0 to 1 have been prepared on ITO substrates. The alloyed nanotubes are composed of many nanocrystals with ZB structure, and the outer diameter and wall thickness are within 270-510nm and 30-80nm, respectively. As the cell constant decreases with addition of Se due to its smaller atom diameter than Te, the band gap of the alloys also presents a nonlinear behavior, which enables $CdSe_{0.30}Te_{0.70}$ and $CdSe_{0.44}Te_{0.56}$ have respective band gap of 1.46 eV and 1.44 eV, much narrower than pure CdSe and CdTe. Raman scattering has been demonstrated for the alloyed nanotubes, in which LO and SO phonon vibrations similar with CdSe and CdTe have been detected. Especially, the intensity of SO mode is much stronger than LO mode for $CdSe_{0.30}Te_{0.70}$ and $CdSe_{0.44}Te_{0.56}$ nanotube arrays due to the alloying compositional disorder related with grain boundaries or defects. Based on the lattice constant changing and Raman vibration shifts, the contributions for the band gap bowing have been demonstrated.

Keywords: Compositional effect, CdSeTe, Nanotube, Raman, Band gap

*Corresponding author. Email: nanoguy@126.com; liquan@phy.cuhk.edu.hk

Introduction

One dimensional (1D) semiconductor nanostructures have attracted research interests due to the superior photoelectronic, catalytic and mechanical properties compared with their thin film or bulk counterparts.[1] Especially, when the 1D nanostructures were grown on electric conducting and optical transparent substrates such as indium or fluorine-doped tin oxide (ITO or FTO) glass substrates, it will be of great potential for various photoelectronic applications including solar cells, solar water splitting and organic photodegradation.[2] Among the various semiconductors, ZnO (TiO_2) nanotube and/or nanorod arrays were most widely studied to serve as electron transfer channels for high efficient sensitized solar cells.[3] In most cases, because of the large band gap of ~3.3eV, they have to be combined or coupled with narrow-gap ones including CdS, CdSe, PbS and CdTe to extend their absorption profiles to cover the visible light region, thus enhancing the devices performance.[4] Though single component nanostructures with narrow gap such as CdSe, CdS, WO_3, Fe_2O_3 have been attempted as photoelectrodes,[5] their response to visible light still located within the wavelength region shorter than 2eV, which greatly limit their further application in photoelectronic devices.

On the other hand, constructing ternary semiconductor alloys (AB_xC_{1-x}) is another efficient way to increase the absorption over visible light.[6] During the alloying process, the compositional effect mainly originates from the strong dependence of the energy level over the effective mass of excitons, which will then affect the absorption and band-edge photoluminescence property of the excitons.[7] For example, it has been demonstrated that the band gaps of PbS_XS_{e1-X} nanocrystals vary linearly with X value, which makes the absorption peak of the alloy locate between those of pure PbS and PbSe.[8] Very differently, an theoretical research showed that according to optical bowing effect, the band gap of $CdSe_XTe_{1-X}$ varies nonlinearly and may be tuned to a value smaller than both CdSe (Eg: 1.7eV) and CdTe (Eg: 1.5eV), i.e. the absorption edge of the CdSeTe alloy can be tuned to infrared region.[7] When combined with the advantages of nanoarrays structure on ITO, it will have more potential applications in photoelectronic devices with response to infrared region. In comparison with CdSSe, ZnSeCd, Zn_2SnO_4, SnO_2, Cu_2ZnSnS_4 and PbSSe,[8, 9] however, there is less report on the synthesis and optical study of the CdSeTe nanotube arrays up to now.

In this work, well-aligned cubic ZB phase $CdSe_XTe_{1-X}$ nanotube arrays with X valued from 0 to1 have been prepared on ITO substrates. The nanotubes are composed of many nanocrystals with cell constant

decreasing with X value. A nonlinear compositional effect based on the absorption property have been found for the alloyed nanotubes, of which $CdSe_{0.30}Te_{0.70}$ and $CdSe_{0.44}Te_{0.56}$ have band gap as narrow as 1.46eV and 1.44 eV, respectively. The Raman property of the $CdSe_XTe_{1-X}$ nanotubes has also been systematically studied based on the alloying compositional effect.

Experimental

Sample Synthesis

The CdSeTe nanotube arrays samples were synthesized via a two-step method using ZnO nanorod array-on-ITO as the template. Firstly, $CdSe_XTe_{1-X}$ was electrodeposited onto ZnO nanorods surface using a three-electrode electrochemical workstation (CH Instrument, model 660C). The ZnO nanorod arrays-on-ITO, Pt foil and a standard saturated calomel electrode (SCE) are used as the working electrode, the counter electrode and the reference electrode, respectively. The electrolyte was composed of 4mM potassium tellurite (K_2TeO_3), sodium selenosulfate (with excess sulfate), 0.05 M nitrilotriacetic acid trisodium salt (NTA), and 0.02 M cadmium acetate. Se/Te source mole ratio was tuned from 0/1, 1/38, 1/19, and 1/6 to achieve CdTe, C_1 ($CdSe_{0.30}Te_{0.70}$), C_2 ($CdSe_{0.44}Te_{0.56}$) and C_3 ($CdSe_{0.77}Te_{0.23}$) alloys, respectively. For pure CdSe, 50mM sodium selenosulfate was used as Se source without addition of Te source. For all the samples, the electrodeposition was performed at a fixed potential of −0.9 V *vs* SCE for 20 minutes. In this step, core–shell ZnO–$CdSe_XTe_{1-X}$ nanocable arrays will be obtained. Secondly, the ZnO–$CdSe_XTe_{1-X}$ nanocable arrays were dipped into 25% (V:V) ammonia aqueous solution for 80 min to completely etch off the ZnO nanorod-cores, leaving $CdSe_XTe_{1-X}$ nanotube arrays standing alone on the ITO substrate. After which, the $CdSe_XTe_{1-X}$ nanotube arrays were annealed at 350°C for 1 h under Ar atmosphere to enhance the crystallinity.

Structural, optical and Raman characterization

The morphology, chemical composition and microstructure of the samples were characterized using field-emission scanning electron microscopy (FE-SEM, FEI Quantum F400) and transmission electron microscopy (TEM, Tecnai 20, FEG, equipped with an energy dispersive X-ray (EDX) spectrometer), and X-ray diffraction (XRD, Ragiku RU300). The optical absorption measurements were performed using a UV-VIS-IR spectrometer (U3501) at room temperature. Raman spectra were recorded with a spectral resolution of $0.5cm^{-1}$ using a Raman system (JY, HR-800) under power of 0.1mW, and the 532 nm line of

Nd^{3+}:YAG laser was used for excitation.

Results and discussion

Figs. 1a-f show the SEM images of the $CdSe_XTe_{1-X}$ nanotube arrays on ITO with variation of X values. As shown by Fig 1 a, b and f, near vertical CdSe and CdTe nanotube arrays can be readily formed by the selective etching of ZnO cores when the ZnO-CdSe or ZnO-CdTe core-shell nanocables were soaked into ammonia solution.[2b] Very similarly, for the alloyed ZnO-$CdSe_XTe_{1-X}$ nanocable arrays samples, the ZnO cores can also be dissolved due to its reaction with ammonia, leaving the $CdSe_XTe_{1-X}$ alloyed nanotube arrays well standing on the ITO substrate (see Figs. 1c-e). Especially, from Figs. 1a-b and the inset, which respectively represent top-show image of the standing and partially lying CdSe nanotubes taken from deliberately destroyed region, it can be clearly seen that the end of CdSe was not totally open. Such phenomena also occur for C_1, C_2 and C_3 alloy nanotube arrays, which mainly come from the different deposition rate of CdSeTe on the top and side surface. The outer diameter and wall thickness of $CdSe_XTe_{1-X}$ nanotubes are within 270-510nm and 30-80nm, respectively, which highly depends on the diameter of ZnO cores and CdSeTe electrodeposition time.

To further confirm the microstructure and X value of the $CdSe_XTe_{1-X}$ nanotube arrays, TEM and the related techniques were performed. Figs 2A-2E and 2a-2e show the low-magnification TEM images, EDX spectra and selective area electron diffraction (SAED) patterns of the CdSe, C_1, C_2, C_3 and CdTe nanotubes, respectively. From Figs 2A-2E, consecutive nanotubes formed for CdSe, CdTe, C_1, C_2 and C_3 samples. The outer diameter and shell thickness of these nanotubes are within 270-510nm and 30-80nm, respectively, well corresponds to the above SEM results. Semi-open or full-open ends can be also clearly found in Fig 2 B, 2E and 2D for C_1, CdTe nanotube and C_3 samples. From the corresponding EDX spectra, when the Se/Te source mole ratio was tuned to 1/6, 1/19 and 1/38, the X value of C_1, C_2 and C_3 can be decided as 0.77, 0.44 and 0.30, respectively. This suggests that the X value increases nonlinearly with the addition of Se source. Interestingly, the X value will cease to change with further increase of Se source once Se/Te source is above 1/6, suggesting that the highest X for the alloyed $CdSe_XTe_{1-X}$ nanotubes is 0.77 using the methods reported by this work. From the SAED patterns of the alloyed nanotubes, diffuse diffraction rings can be observed indicating that the nanotubes are mainly polycrystalline, while the bright diffraction dots along these rings show that there are many single-crystalline nanocrystals mingled with the nanotubes. For both CdSe and

CdTe nanotubes, three diffraction rings marked by white lines appear from the inside radically outside, which can be indexed to (111), (220), and (311) planes of cubic zinc-blend (ZB) structure of CdSe and CdTe. Considering that the interplane distance (d) is equal to constant a divided by the ring diameter (R),[11] the rings diameter should become smaller with the decrease of X because that the lattice constant of the alloyed nanotubes gets bigger with the increase of Te content . However, there are not obvious differences in the rings diameter of the alloys since the rings are very diffuse with many big and bright diffraction dots.

The crystalline structure of the $CdSe_XTe_{1-X}$ alloyed nanotube arrays were further studied by XRD technique as shown by Fig. 3. The diffraction peaks from ITO substrate were marked with cross, and the ZnO signals (labeled with an asterisk) came from ZnO underlayer which served as seed layer for the growth of ZnO nanorods. This underlayer remains unchangeable in spite of the etching of the ZnO nanorod cores by ammonia. The diffraction peaks of the $CdSe_XTe_{1-X}$ alloyed nanotubes were summarized in Table 1, which shows that the reflection peaks at 25.384º, 41.981º and 49.646º correspond well with the (111), (220) and (311) planes of cubic ZB CdSe (PDF card No. 88-2346). The peak at 24.053º indicates that partial transition of cubic ZB to hexagonal wurtzite phase occurs for CdSe due to the annealing process at 350º.[10] With the increase of Te content, the peaks of (111), (220) and (311) planes get smaller gradually for the alloys. Until X equals to 0, the peaks can be indexed to the cubic ZB phase of CdTe (PDF No. 65-880). Therefore, the $CdSe_XTe_{1-X}$ alloyed nanotubes have a main structure of cubic ZB, which is consistent with the SAED results. According to Scherrer equation, the average grain sizes are 41.9, 34.1, 30.4, 32.4 and 42.8 nm for CdSe, $CdSe_{0.77}Te_{0.23}$, $CdSe_{0.44}Te_{0.56}$, $CdSe_{0.30}Te_{0.70}$, and CdTe alloys, respectively. No obvious peaks of CdSe or CdTe appear in the XRD patterns of the alloys, suggesting that there are not obvious phase separations among the alloys. However, the possibility of partial mixture of CdSe and CdTe grains can not be completely excluded.

The cell constants of the $CdSe_XTe_{1-X}$ nanotube alloys can be estimated from Bragg formula ($2d\sin\theta=\lambda$) and Vegard's law ($a=X\bullet a_1+(1-X)\bullet a_2$), respectively.[12] The wavelength λ of Cu Kα1 is 1.5406Å, the interplane distance d can be decided from constant a divided by $(h^2+k^2+l^2)^{1/2}$ (here (hkl) adopts (220) plane due to its high intensity in the XRD patterns), and a_1 and a_2 represents the calculated cell constant of pure CdSe (6.082Å) and CdTe (6.476Å) from Bragg equation, respectively. As shown by Figure 3b, the calculated lattice constant a decreases with X resulting from the substitution of larger Te atoms with smaller Se atoms. The deviation of the calculated values from the two methods is less than 2%, suggesting that X values

measured from the EDX measurements are reasonable. The lattice compression is 9.1%, 39.6% and 94.4% for the respective alloy with X of 0.30, 0.44 and 0.77 in comparison to CdTe.

Table 1 Two-theta positions indexed to the crystal planes of the $CdSe_XTe_{1-X}$ alloyd nanotube arrays

Indexed plane	CdSe (°)	$CdSe_{0.77}Te_{0.23}$ (°)	$CdSe_{0.44}Te_{0.56}$ (°)	$CdSe_{0.30}Te_{0.70}$ (°)	CdTe (°)
(111)	25.384	25.230	24.372	23.900	23.790
(220)	41.981	41.827	40.331	39.550	39.320
(311)	49.646	49.338	47.534	46.677	46.430

The compositional effect on the absorption property of the $CdSe_XTe_{1-X}$ nanotube alloys was further studied. As shown by Fig. 4, pure CdTe nanotube arrays have an absorption edge at ~810 nm, well consistent with its band gap of 1.54eV. The absorption edges for pure CdSe locates at 740nm, which has little blue-shifted compared to the band gap (1.74eV) of bulk CdSe. For $CdSe_{0.77}Te_{0.23}$, the absorption edge is about 760nm, which is between those of CdSe and CdTe. With further addition of Te, the absorption edge of $CdSe_{0.44}Te_{0.56}$ moves to ~864nm, then it slightly blue shifts to ~ 852nm for $CdSe_{0.30}Te_{0.70}$, indicating band gap of 1.44 eV and 1.46 eV for $CdSe_{0.44}Te_{0.56}$ and $CdSe_{0.30}Te_{0.70}$, respectively. Such a result shows that the band edge of both $CdSe_{0.44}Te_{0.56}$ and $CdSe_{0.30}Te_{0.70}$ can be tuned to much wider wavelength range than pure CdTe, which agrees well with the theoretical prediction made by Kamat.[7] The band gap reaches to the narrowest when the Te content is 0.56, which is extremely consistent with that of CdSeTe alloy quantum dots (QDs), in which the Te content is 0.54.[11] As suggested by Bernard and Zunger, the band gap bowing for ZnS, ZnSe, ZnTe and their alloys arises from three contributions including (i) the volume deformation resulted from the lattice constant changing which alters the band structure; (ii) deformed electron distribution due to the electronegativity difference of the alloy elements; and (iii) structural relaxation of the anion-cation bond lengths and angles to accommodate the atoms with various size.[13] In the case of $CdSe_{0.30}Te_{0.70}$, the lattice compression is only 9.1%, which indicates that the band gap bowing is attributed to the electronic factors. With X increasing to 0.44 or higher, the structure contribution due to the lattice constant changing or/and bond length may dominates the band gap bowing.

Raman scattering is another powerful tool to study the influence of elemental composition and cell constant on the lattice vibration of alloys. Simultaneously, the good crystalline property makes it valuable to study the Raman property of the alloyed $CdSe_XTe_{1-X}$ nanotube arrays. Fig. 5 shows the typical Raman spectra for pure CdTe, CdSe and ternary $CdSe_XTe_{1-X}$ nanotube arrays. For pure CdTe nanotubes, the peaks at

~123 cm^{-1} and 165 cm^{-1} can be attributed to Te acoustic (A_1) and CdTe longitudinal optical (LO) phonon mode, respectively.[14] Because of the overlapping property of the Te E at ~139cm^{-1} and CdTe transverse optical (TO) phonon at ~141 cm^{-1}, the Raman shift at 142 cm^{-1} could be a contribution from both Te and CdTe TO.[15] Compared with the LO phonon frequency ranges from 170cm^{-1} to 173cm^{-1} for bulk CdTe, the red shift of the LO vibration here originates from phonon confinement effect reported for semiconductor nanoparticles. The signals of Te E and A_1 mode indicate that there exist Te inclusions or defects around the grain boundaries of CdTe nanocrystals,[14a, 16] which maybe caused by the preparation method used in this work. Note that the amount of Te inclusions or defects can not be quantified from the Raman measurements since that Te crystals exhibit a rather high Raman scattering ability compared with CdTe due to the unequal Raman cross sections.[17]

For pure CdSe nanotube arrays, two peaks present at 192 cm^{-1} and 206 cm^{-1}, respectively, which can be assigned to the surface optical (SO) and LO phonon of CdSe.[17] The presence of SO scattering is mainly due to a symmetry broken associated with surface roughness of the polycrystalline CdSe nanotubes, which were mainly composed of many nanocrystals.[18] With addition of Se, the CdTe LO peak is weaken greatly with the appearance of the peak located at ~192 cm^{-1} for ternary $CdSe_{0.30}Te_{0.70}$ nanotubes, which maybe originated from the SO phonon mode. At the same time, Te inclusions or defects still exist in the nanotubes. Until Se content is increased to 44% for $CdSe_{0.44}Te_{0.56}$ nanotubes, little signal from Te inclusions could be found in the spectrum. In addition, two Raman peaks appear at 142 cm^{-1} and 159 cm^{-1}, which can be respectively assigned to TO and SO phonon of CdTe.[14] At higher frequency region, two peaks related with SO and LO-like CdSe vibration also appear at 190cm^{-1} and 203 cm^{-1}, respectively. Such a result suggests that both Cd-Se and Cd-Te vibrations dominate in the sample. When Se content increases up to 0.77, only SO and LO-like CdSe peak can be detected.

Except the acoustic mode of Te and TO vibration of CdTe, the spectra of the above $CdSe_XTe_{1-X}$ alloys are very similar. The location of LO mode of $CdSe_XTe_{1-X}$ upshifts to longer wavenumber with increase of x due to the shortened cell constant. It is clear that for $CdSe_{0.30}Te_{0.70}$ and $CdSe_{0.44}Te_{0.56}$, the intensity of SO vibration mode is stronger than the LO mode, which can be attributed to the increased alloying compositional disorder with more grain boundaries or defects.[19] Additionally, the CdSe LO vibration slightly downshifts for $1>X \geq 0.44$ due to the shortened lattice constant, which also suggests that the band gap bowing for the nanotube alloys with $X \geq 0.44$ arises from the structure contribution associated with lattice

constant changing or/and bond length.

Conclusions

In summary, well-aligned $CdSe_XTe_{1-X}$ nanotube arrays with X ranged from 0 to 1 were prepared on ITO substrates. The alloyed nanotubes are composed of many nanocrystals with ZB structure, and the cell constant decreases with X increasing because of the substitution of larger Te atoms with smaller Se atoms. The band gap of the alloys varies nonlinearly with X, which makes $CdSe_{0.30}Te_{0.70}$ and $CdSe_{0.44}Te_{0.56}$ have narrow band gap than pure CdSe and CdTe due to compositional effect. Both the LO and SO phonon vibrations similar with CdSe and CdTe have been detected for the alloys. Especially, because of the alloying compositional disorder related with grain boundaries or defects, the intensity of SO mode is much stronger than LO mode for $CdSe_{0.30}Te_{0.70}$ and $CdSe_{0.44}Te_{0.56}$ nanotube arrays. Both the lattice constant changing and the LO vibration shifts suggest that the band gap bowing for the alloys with $X \geq 0.44$ arises from the structure contribution associated with lattice constant changing or/and bond length.

Acknowledgments

This work was supported in part by the National Nature Science Foundation of China (No.51372075, 51472080), Research Fund for the Doctoral Program of Higher Education of China (RFDP, No. 20104208120004), and Wuhan Youth Chenguang Program of Science and Technology under Grant No. 2013070104010014.

References

1 *(a)* K. Zhu, N. R. Neale, A. Miedaner and A. J. Frank, *Nano Lett.,* 2007, **7**, 69; *(b)* P. A. Sergiu, G. Andrei, M. Jan, H. Robert and S. Patrik, *Nano Lett.,* 2007, **7,** 1286; *(c)* M. H. Huang, S. Mao, H. Feick, H. Q. Yan, Y. Y. Wu, H. Kind, E. Weber, R. Russo and P. D. Yang, *Science,* 2001, **292**, 1897; *(d)* Y. Cui, Q. Q. Wei, H. K. Park and C. M. Lieber, *Science,* 2001, **293**, 1289; *(e)* Z. W. Pan, Z. R. Dai and Z. L. Wang, *Science,* 2001, **291**, 1947.

2 *(a)* J. Zhang, S. Q. Li, H. Ding, Q. T. Li, B. Y. Wang, X. N. Wan and H. Wang, *J. Power Sources,* 20142, **47**, 807; *(b)* X. N. Wang, G. S. Li, H. J. Zhu, Y. C. Yu, X. D. Xiao and Q. Li, *Appl. Catal. B: Envir.,* 2014, **147**, 17; *(c)* G. Wang, H. Wang, Y. Ling, Y. Tang, X. Yang, R. C. Fitzmorris, C. Wang, J. Z. Zhang and Y. Li, *Nano Lett.,* 2011, **11**, 3026.

3 (a) D. Kuang, J. Brillet, P. Chen, M. Takata, S. Uchida, H. Miura, K. Sumioka, S. M. Zakeeruddin and M. Gra¨tzel, *ACS Nano* 2008, **2**, 1113; *(b)* A. B. F. Martinson, J. W. Elam, J. T. Hupp, and M. J. Pellin, *Nano Lett.* 2007, **7**, 2183; *(c)* T. S. Kang, A. P. Smith, B. E. Taylor and M. F. Durstock, *Nano Lett.* 2009, **9**, 601; *(d)* C. H. Ku, and J. J. Wu, *Appl. Phys. Lett.* 2007, **91**, 093117; *(e)* K. Shankar, J. Bandara, M. Paulose, H. Wietasch, O. M. Varghese, G. K. Mor, T. J. LaTempa, M. Thelakkat and C. A. Grimes, *Nano Lett.,* 2008, **8**, 1654.

4 *(a)* W. T. Sun, Y. Yu, H. Y. Pan, X. F. Gao, Q. Chen and L. M. Peng, *J. Am. Chem. Soc.,* 2008, **130**, 1124; *(b)*K. S. Leschkies, R. Divakar, J. Basu, E.Enache-Pommer, J. E. Boercker, C. B. Carter, U. R. Kortshagen, D. J. Norris and E. S.

Aydil, *Nano Lett.,* 2007, **7**, 1793; *(c)* R. Plass, P. Serge, J. Kruger, M. Gra¨tzel and U. Bach, *J. Phys. Chem. B* 2002, **106**, 7578.

5 *(a)* E. Elmalem, A. E. Saunder, R. Costi, A. Salant and U. Banin, *Adv. Mater.,* 2008, **20**, 4312; *(b)* B. Cao, Y. Jiang, C. Wang, W. Wang, L. Wang, M. Niu, W. Zhang, Y. Li and S. T. Lee, *Adv. Func. Mater.,* 2007, **17**, 1501; *(c)* P. M. Rao, L. Cai, C. Liu, I. S. Cho, C. H. Lee, J. M. Weisse, P. Yang and X. Zheng, *Nano Lett.,* 2014, **14**, 1099; *(d)* J. Li, S. K. Cushing, P. Zheng, F. Meng, D. Chu and N. Wu, *Nat. Comm.,* 2013, **4**, 3651.

6 J. Xu, X. Yang, H. Wang, X. Chen, C. Luan, Z. Xu, Z. Lu, V. A. L. Roy, W. Zhang and X. Lee, *Nano Lett.,* 2011, **11**, 4138.

7 P. K. Santra and P. V. Kamat, *J. Am. Chem. Soc*., 2012, **134**, 25058.

8 *(a)*W. Ma, J. M. Luther, H. Zheng, Y. Wu and A. P. Alivisatos, *Nano Lett.,* 2009, **9**, 1699; *(b)* L. Shi and Y. Dai, *J. Mater. Chem. A,* 2013, **1**, 12981; *(c)* L. Shi, Y. Xu, Q. Li, *Nanoscale,* 2010, **2**, 2104; *(d)* L. Shi, C. J. Pei, Y. Xu, Q. Li, *J. Am. Chem. Soc.,* 2011, **133**, 10328.

9 T. P. A. Ruberu and J. Vela, *ACS Nano*, 2011, **5**, 5775.

10 R. Tena-Zaera, A. Katty, S. Bastide and C. Levy-Clement, *Chem. Mater.,* 2007, **19**, 1626.

11 B. Hou, D. Parker, G. P. Kissling, J. A. Jones, D. Cherns and D. J. Fermin, *J. Phys. Chem. C*, 2013, **117**, 6814.

12 Y. M. Sung, Y. J. Lee and K. S. Park, *J. Am. Chem. Soc.,* 2006, **128**, 9002.

13 J. E .Bernard and A. Zunger, *Phys. Rev. B* 1987, **36**, 3199.

14 *(a)* V. S. Vinogradov, G. Karczewski, I. V. Kucherenko, N. N. Melnik and P. Fernandez, *Phys. Solid State,* 2008, **50**, 164; *(b)* P. M. Amirtharaj and F. H. Pollak, *Appl. Phys. Lett.,* 1984, **45**, 789.

15 V. Dzhagan, M. Ya. Valakh, J. Kolny-Olesiak, I. Lokteva and D. R. Zahn, *Appl. Phys. Lett.,* 2009, **94**, 243101.

16 J. S. Mak, A. A. Farah, F. Chen and A. S. Helmy, *ACS Nano,* 2011, **5**, 3823.

17 (a) S. A. Rutledge, A. A. Farah, J. Dinglasan, D. J. Anderson, A. Das, J. Goh, C. Goh and A. S. Helmy, *J. Phys. Chem. C,* 2009, **113,** 20208; *(b)* N. Tschirner, H. Lange, A. Schliwa, A. Biermann, C. Thomsen, K. Lambert, R. Gomes and Z. Hens, *Chem. Mater.* 2012, **24**, 311.

18 L. Xi, K. H. Chua, Y. Zhao, J. Zhang, Q. Xiong, Y. M. Lam, RSC Advances, 2012, 2, 5243-5253.

19 B. Cheng, J. Jiao, W. Sun, B. Tian, Y. Xiao, S. Lei, *Nanotech.* 2010, **21**, 025704.

Figure Captions

Figure 1 SEM images of CdSe (a and b with different magnification), $CdSe_XTe_{1-X}$ alloy C1(c), C2(d), C3(e), and CdTe (f) nanotube arrays on ITO substrate. The inset in Fig1a shows some lying CdSe nanotubes taken from deliberately destroyed region.

Figure 2 Low-magnification TEM images, EDX spectra and the corresponding SAED patterns of CdSe (A, a), C1 ($CdSe_{0.77}Te_{0.23}$, B, b), C2 ($CdSe_{0.44}Te_{0.56}$, C, c), C3 ($CdSe_{0.30}Te_{0.70}$, D, d), and CdTe (E, e) nanotubes.

Figure 3 XRD patterns of the $CdSe_XTe_{1-X}$ nanotube arrays (a), and lattice constant a as function of Se content X extracted from Bragg equation and Vegard law, respectively.

Figure 4 Absorption spectra of CdSe, $CdSe_{0.77}Te_{0.23}$, $CdSe_{0.44}Te_{0.56}$, $CdSe_{0.30}Te_{0.70}$, and CdTe nanotube arrays. The absorption edges for above samples are located at 740, 760, 864, 852 and 810 nm, respectively.

Figure 5 Raman spectra of CdSe, $CdSe_{0.77}Te_{0.23}$, $CdSe_{0.44}Te_{0.56}$, $CdSe_{0.30}Te_{0.70}$, and CdTe nanotube arrays. Detailed Raman shifts have been marked around the corresponding peaks for clarity.

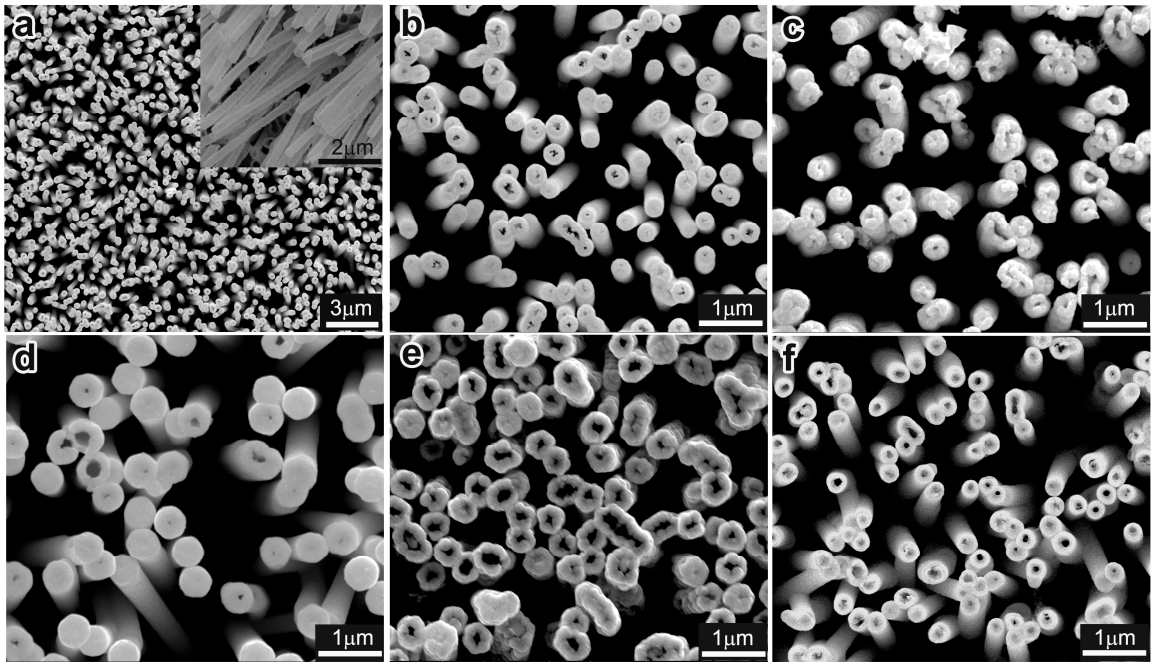

Fig. 1

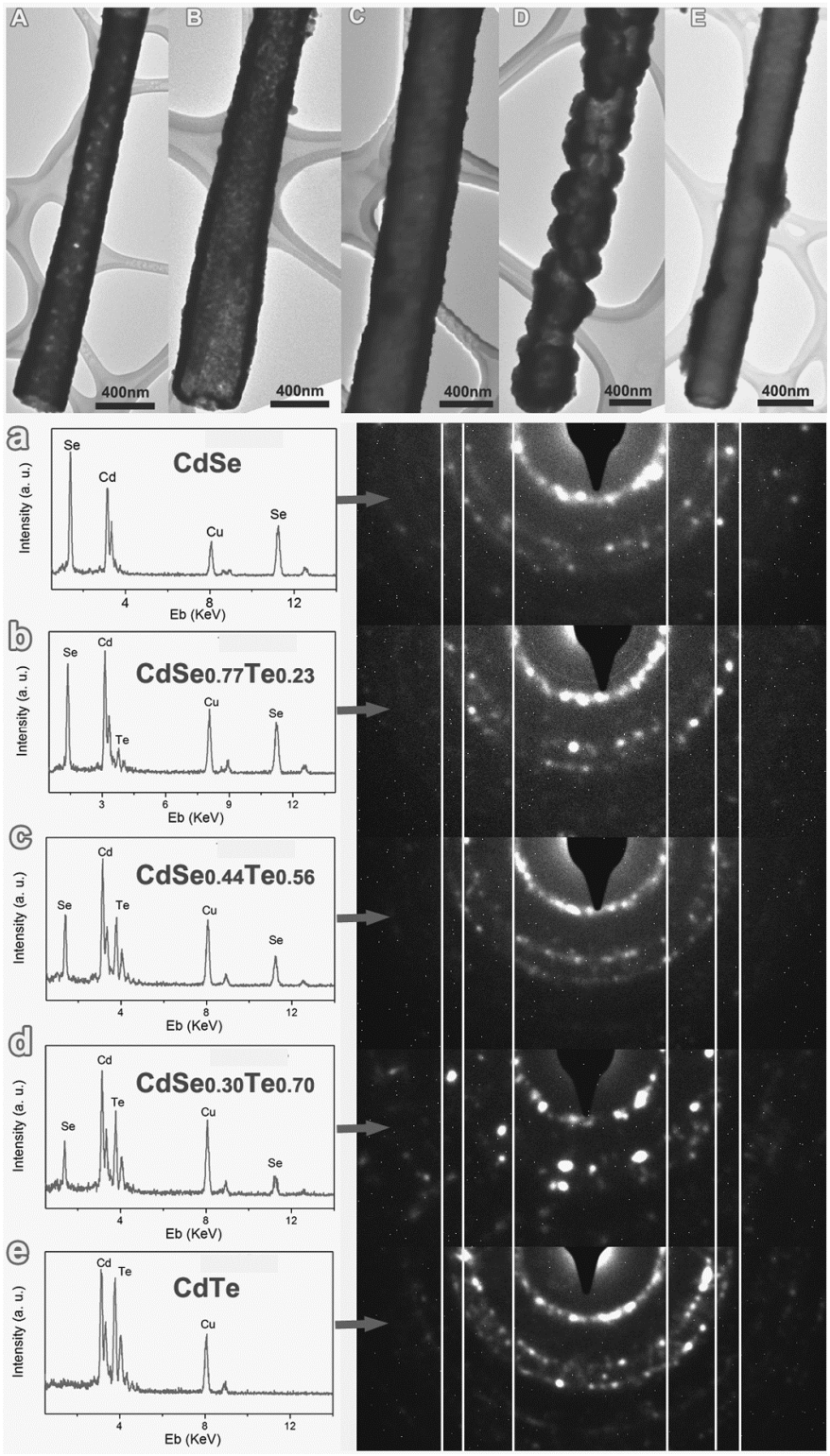

Fig. 2

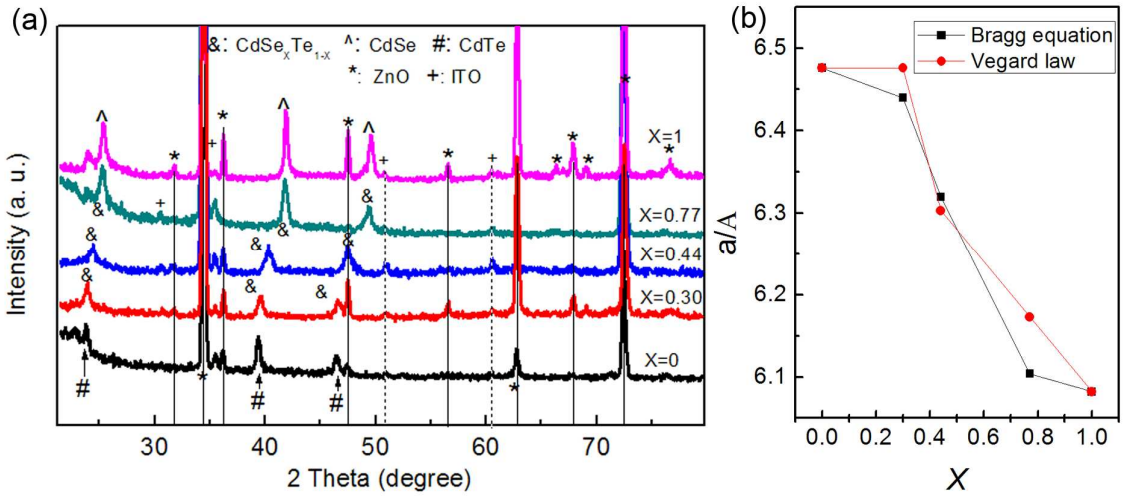

Fig. 3

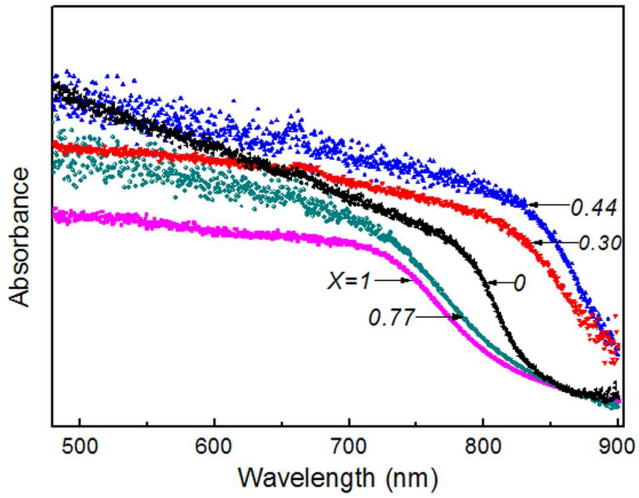

Fig. 4

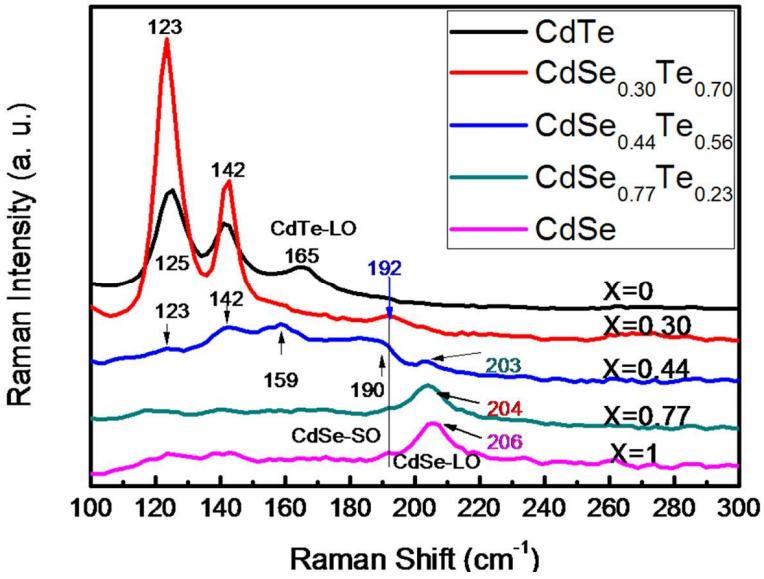

Fig. 5

Compositional effects and optical properties of $CdSe_XTe_{1-X}$ alloyed nanotube arrays

Xina Wang,[1, 2] Yang Xu,[1] Rui Tong,[1] Xiaolong Zhou,[1] Quan Li,[2,*] Hao Wang[1,*]

[1]*Hubei Collaborative Innovation Center for Advanced Organic Chemical Materials, Faculty of Physics and Electronic Technology, Hubei University, Wuhan, Hubei 430062*

[2]*Department of Physics, The Chinese University of Hong Kong, Shatin, New Territory, Hong Kong, China,*

For Table of Contents Use Only

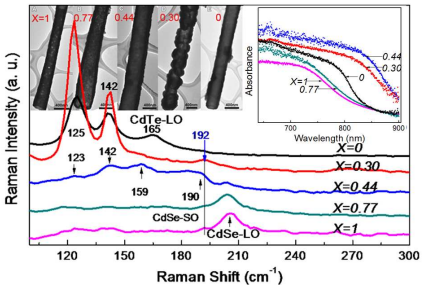

The compositional effects on cell constant, absorption and Raman scattering were demonstrated for well-aligned $CdSe_XTe_{1-X}$ ($0 \leq X \leq 1$) nanotube arrays on ITO.

*Corresponding author. Email: nanoguy@126.com; liquan@phy.cuhk.edu.hk